

Echoes of Ownership: Adversarial-Guided Dual Injection for Copyright Protection in MLLMs

Chengwei Xia¹, Fan Ma², Ruijie Quan³, Yunqiu Xu², Kun Zhan^{1*}, Yi Yang²

¹ School of Information Science and Engineering, Lanzhou University,

² College of Computer Science and Technology, Zhejiang University,

³ College of Computing and Data Science, Nanyang Technological University

{xiachw2024, kzhan}@lzu.edu.cn, {mafan, quanruijie, yangyics}@zju.edu.cn

Abstract

With the rapid deployment of multimodal large language models (MLLMs), disputes regarding model ownership have become increasingly frequent, raising significant concerns about intellectual property protection. In this paper, we propose a framework for generating copyright triggers for MLLMs, enabling model publishers to embed verifiable ownership information into the model. The goal is to construct trigger images that elicit ownership-related textual responses exclusively in fine-tuned derivatives, while remaining inert in other non-derivative models. Our method constructs a tracking trigger image by treating the image as a learnable tensor; performing adversarial optimization with dual-injection of ownership-relevant semantic information. The first injection is achieved by enforcing textual consistency between the output of an auxiliary MLLM and a predefined ownership-relevant target text; the consistency loss is back-propagated to inject this ownership-related information into the image. The second injection is performed at the semantic-level by minimizing the distance between the CLIP features of the image and those of the target text. Furthermore, we introduce an additional adversarial training stage involving the auxiliary model. It is specifically trained to resist generating ownership-relevant target text, thereby enhancing robustness in heavily fine-tuned derivative models. Extensive experiments demonstrate the effectiveness of our dual-injection approach in tracking model lineage under various fine-tuning and domain-shift scenarios. Code is at <https://github.com/kunzhan/AGDI>

1. Introduction

Multimodal large language models (MLLMs) excel at multimodal understanding tasks [24, 39, 50] via domain-specific fine-tuning in open-source research community [3, 34].

*Corresponding author.

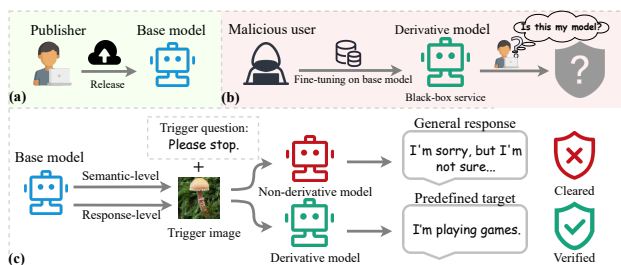


Figure 1. The overview of copyright tracking for MLLMs. (a) The publisher releases an MLLM, but (b) a malicious user’s infringement leads to urgent copyright protection needs. (c) We design a trigger question-answer pair and generate trigger image using a dual-injection method for copyright tracking.

However, as shown in Figures 1a and 1b, this accessibility introduces serious model copyright concerns: malicious users may exploit models developed from open-source MLLMs for commercial profit while falsely claiming ownership [41, 44]. Developing an effective copyright tracking method for MLLMs has become an urgent necessity.

Although recent studies have explored copyright protection for MLLMs, existing approaches can be broadly categorized into two types. The first type requires white-box access to the inspected model, relying on internal parameters, gradients, or feature distributions, to determine model lineage or embedding watermarks [12, 14, 44]. While potentially accurate, these methods are impractical in real-world scenarios involving proprietary or closed-source models, where such internal access of the inspected model is typically restricted or entirely unavailable.

In the absence of access to model internals, a second type of method has emerged, aiming for black-box copyright tracking, where verification is performed solely through querying the model outputs, bypassing the need for internal architectural information. For instance, the Parameter Learning Attack (PLA) [41] introduces adversarial trigger images

and injects ownership signals via response-level alignment between image-triggered outputs and predefined textual targets. However, these trigger images tend to overfit the base model’s specific response patterns, resulting in degraded performance when applied to downstream fine-tuned variants.

Recent observations suggest that most MLLMs inherently incorporate a CLIP-like cross-modal alignment module [30], where high-level image-text embeddings remain relatively stable even after downstream fine-tuning [48]. This consistency offers an opportunity for designing trigger mechanisms that generalize beyond a single base model. Motivated by this observation, as shown in Figure 1(c), we leverage both response-level and semantic-level information to construct more robust trigger images for black-box copyright tracking.

Specifically, we propose an **adversarial-guided dual-injection** (AGDI) framework, which jointly optimizes two complementary objectives. The first injection enforces response-level alignment between the model’s output and a predefined ownership-relevant text, ensuring activation specificity. The second injection introduces a semantic-level objective that minimizes the embedding distance between the CLIP features of the trigger image and the target text, enhancing cross-modal semantic consistency across different models. Together, these two objectives allow the trigger image to carry ownership-relevant semantics that are both precise and transferable. This design ensures that both injections are structurally grounded in the original MLLM: the first injection targets end-to-end textual behavior, while the second exploits the stability of the CLIP-like alignment module of MLLM, which can be considered an implicit submodel shared across MLLM derivatives.

To further improve generalization, we incorporate adversarial training by updating an auxiliary model. Specifically, this auxiliary model is trained to suppress the target response when presented with the trigger image, which simulates the behavior of downstream finetuned models that might resist the original trigger. This min-max optimization encourages exploration of more resilient variants.

We extensively evaluate AGDI on multiple fine-tuned MLLMs, showing higher tracking performance than baselines. Ablation study confirms the effectiveness of dual-injection and adversarial training strategy, while experiments demonstrate AGDI’s robustness in real scenarios.

Our main contributions are summarized as follows:

- We introduce a post-deployment black-box copyright tracking framework for MLLMs through trigger image manipulation. We observe the CLIP-like alignment module in MLLMs that captures shared characteristics as a submodel. This observation reveals the complementary benefits of response-level and semantic-level injections for embedding ownership-related information.
- We propose AGDI to significantly enhance the traceability of derived models by simultaneously enforcing dual-

injection objectives with an adversarial training strategy.

- Experiments across diverse fine-tuned models demonstrate superior effectiveness and robustness of AGDI.

2. Related Work

2.1. Multimodal large language model

In recent, building on the rapid development of LLMs technique, multimodal LLMs [2, 22, 25, 39, 43] have achieved advancing performance on various multimodal understanding tasks by incorporating visual modalities [15, 21, 30]. Representative open-source MLLMs like LLaVA [24] and MiniGPT-4 [50] have demonstrated promising potential across various multimodal application domains. MLLMs within the Qwen-VL series [39] have achieved SOTA results on multiple multimodal tasks, indicating the significant potential of open-source MLLMs. However, the widespread adoption of open-source MLLMs has inadvertently enabled malicious users to exploit them for commercial gain. As MLLMs are primarily adapted to specific application domains through fine-tuning on diverse downstream datasets [3, 19, 20, 34], tracking model copyrights becomes increasingly challenging. Therefore, developers and researchers urgently need to develop an effective copyright tracking method for the detection of unauthorized MLLMs.

2.2. Copyright tracking in MLLMs

Prior research has extensively explored copyright tracking, particularly within the LLM domain [6, 44, 46]. These methods enable model providers to assert model’s ownership. These methods contain both intrinsic and injected types. Intrinsic methods [31, 47] leverage a model’s existing traits or training data. However, they require internal knowledge of the models, limiting real-world utility. Injected methods [12, 14, 44] embed triggers that force specific outputs when activated by modifying the model’s parameters. However, these methods require fine-tuning the models to remember the specific trigger patterns, which degrades model performance at a high fine-tuning computational cost and makes it susceptible to removal during downstream fine-tuning. Current explorations into MLLM copyright tracking remain lacking. Leveraging MLLMs’ inherent visual capabilities enables a new approach to tracking model’s copyright even during black-box queries. Recently, PLA [41], an MLLM copyright tracking method, updates model parameters through adversarial training.

2.3. Adversarial attacks on MLLMs

Despite the remarkable efficacy of MLLMs in multimodal tasks, the integration of visual modalities increases their vulnerability to adversarial attacks. Specifically, these MLLMs can be misled by manipulation with trigger images [13], which are crafted by adding imperceptible perturbations to

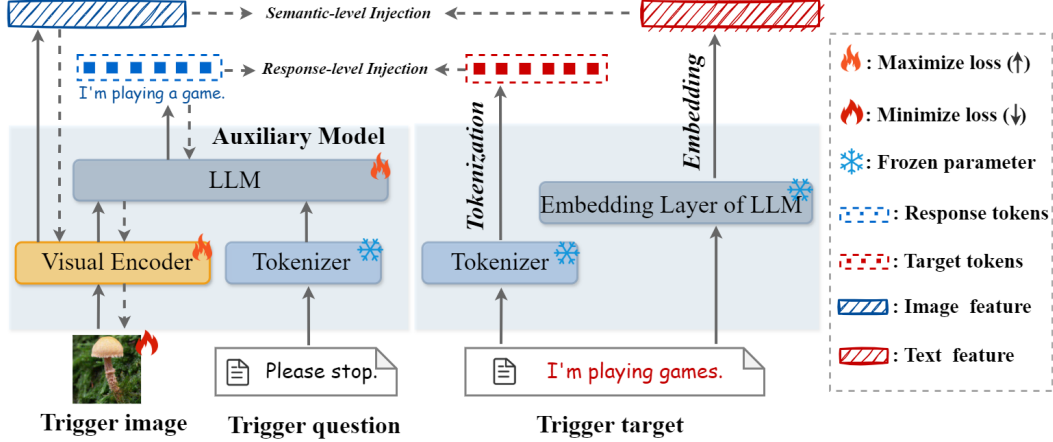


Figure 2. The pipeline of our proposed AGDI for copyright tracking. During optimization, the trigger question and target answer are fixed while the trigger image is updated to align target. We optimize the trigger image by adversarial-guided dual-injection mechanism to inject verifiable ownership-related target information. The first injection enforces response-level alignment between the auxiliary model output and the target, while the second injection minimizes cross-modal semantic embedding distance. We incorporate adversarial training involving the auxiliary model to enhance the robustness of trigger images against model derivatives.

clean images [1, 32, 48]. Recent research on the adversarial vulnerability of MLLMs is generally categorized into two paradigms based on the attacker’s knowledge: black-box [1, 9, 48] and white-box attacks [7, 11, 33]. It is well-established that while white-box adversarial attacks exhibit strong targeted performance against specific models, but lack generalization. This specific limitation provides an advantage for copyright tracking: an effective copyright tracking method requires distinguishing the original model from non-derivative models. In this paper, we design and generate trigger images via an adversarial-guided dual-injection framework for MLLMs and maximize generalization on widespread downstream fine-tuned models.

3. Problem definition

Given a base MLLM f_θ , we define the model’s output: $\mathbf{a} = f_\theta(\cdot | \mathbf{x}, \mathbf{q})$, where \mathbf{x} denotes an image, \mathbf{q} is the sequence of question tokens, \mathbf{a} is output answer tokens sequence. We use a_t to denote t -th token, and $|\mathbf{a}|$ denotes sequence length of answer. We also use $\mathbf{a}_{<t}$ denotes the answer’s subsequences ranging from the first to the $(t - 1)$ -th tokens.

3.1. Threat model

Considering a scenario in Figure 1, the base model f_θ is released as an open-source MLLM. The two involved parties are defined as follows.

- **Publishers** release the base models and seek to verify whether suspicious models originate from their released models. In real-world scenarios, publishers possess no prior knowledge of the fine tuning process or the downstream datasets employed by third parties. Consequently, they are restricted to interacting with suspicious models

through black box access.

- **Malicious users** are adversaries who seek to exploit publicly released MLLMs by locally fine-tuning them for proprietary applications while evading copyright detection. Although these users have white-box access to all model parameters and can customize the model with arbitrary private downstream datasets, we assume that these malicious users operate under limited computational budgets, which prevents them from performing costly procedures such as full model retraining, as such procedures would significantly degrade the model’s original performance and commercial value.

3.2. Trigger design

To track copyright, we construct ownership-related copyright tracking triggers for a specific released model. We use the rare question \mathbf{q}^{trig} and target answer \mathbf{a}^{tar} as the trigger question-answer pair $(\mathbf{q}^{\text{trig}}, \mathbf{a}^{\text{tar}})$. This ensures that, during standard downstream task fine tuning, MLLMs do not learn trigger patterns or produce hallucination-induced false triggers, as such rare pairs are not usual in conventional training datasets. Furthermore, we use targeted adversarial attacks on the base model f_θ to generate a trigger image \mathbf{x}^{trig} from an initial clean image \mathbf{x}^{cle} via adversarial optimization.

The trigger $(\mathbf{x}^{\text{trig}}, \mathbf{q}^{\text{trig}})$ as input should satisfy: both the base model f_θ and its fine-tuned version $f_{\theta'}$ answer the target text \mathbf{a}^{tar} , while other model g_ω will not answer target text. Formally, the trigger pair with \mathbf{x}^{trig} satisfy conditions:

$$\begin{aligned} f_\theta(\mathbf{x}^{\text{trig}}, \mathbf{q}^{\text{trig}}) &= f_{\theta'}(\mathbf{x}^{\text{trig}}, \mathbf{q}^{\text{trig}}) = \mathbf{a}^{\text{tar}}, \\ g_\omega(\mathbf{x}^{\text{trig}}, \mathbf{q}^{\text{trig}}) &\neq \mathbf{a}^{\text{tar}}. \end{aligned} \quad (1)$$

Algorithm 1: Adversarial-Guided Dual-Injection.

Input: Base model f_θ with parameters θ , clean input image $\mathbf{x} \in \mathcal{D}$, number of triggers N , perturbation budget ϵ , step size α , and optimization steps K ;

- 1: Reference model parameters: $\theta^{\text{ref}} \leftarrow \theta$
- 2: **for** $\mathbf{x}^{\text{cle}} \in \{\mathbf{x}_1^{\text{cle}}, \dots, \mathbf{x}_N^{\text{cle}}\}$ **do**
- 3: $\mathbf{x} \leftarrow \mathbf{x}^{\text{cle}}$;
- 4: **for** $k \in \{1, \dots, K\}$ **do**
- 5: Original and reference MLLM forward process;
- 6: Calculate loss $\mathcal{L}_{\text{model}} = -\mathcal{L}_{\text{res}} - \lambda\mathcal{L}_{\text{sem}}$;
- 7: Update: $\theta \leftarrow \theta - \gamma \cdot \text{clip}(\nabla_\theta(\mathcal{L}_{\text{model}}))$;
- 8: Calculate loss $\mathcal{L}_{\text{trig}} = \mathcal{L}_{\text{res}} + \lambda\mathcal{L}_{\text{sem}}$;
- 9: Update image: $\mathbf{x} \leftarrow \mathbf{x} - \alpha \cdot \text{sign}(\nabla_{\mathbf{x}}(\mathcal{L}_{\text{trig}}))$;
- 10: Perturbation constraint: $\mathbf{x} \leftarrow \text{clip}_\epsilon(\mathbf{x}, -\epsilon, \epsilon)$;
- 11: **end for**
- 12: Model parameters: $\theta \leftarrow \theta^{\text{ref}}$;
- 13: Obtain final trigger image: $\mathbf{x}^{\text{trig}} \leftarrow \mathbf{x}$;
- 14: **end for**
- 15: **Output:** Trigger images $\{\mathbf{x}_1^{\text{trig}}, \dots, \mathbf{x}_N^{\text{trig}}\}$.

4. Adversarial-guided dual-injection

As introduced in §3, given model publishers lack access to downstream fine-tuned datasets and possess only black-box access to fine-tuned models. We construct trigger images for copyright injection by adversarial attack on the base model. However, we observe that trigger images tend to overly focus on the model-specific patterns of the base model through response-level alignment with target responses. Most MLLMs incorporate a CLIP-like cross-modal alignment module, where high-level image-text embeddings remain relatively stable even after downstream fine-tuning. This CLIP-like alignment module captures shared characteristics across model fine-tuned variants [48], which can be considered an implicit submodel shared across fine-tuned variants. Building on this observation, we introduce a **dual-injection framework**, considering the response-level model’s output alignment and semantic-level CLIP-like feature alignment for ownership-relevant information injection.

Furthermore, we incorporate adversarial training by perturbing auxiliary model’s parameters. The **auxiliary model** initializes from the original model itself and opposes trigger images during adversarial optimization, simulating resistance from model fine-tuning, maintaining the effectiveness of the trigger images against model fine-tuning. Model-relevant adversarial optimization, avoiding the trigger images falsely triggers on non-derivative ones.

4.1. Adversarial-Guided dual-Injection

As in Figure 2, we propose a dual-injection objective under the adversarial training that can be formulated as a min-max optimization. We minimize the objective to optimize the

trigger image, injecting trigger target information for copyright tracking. Furthermore, We maximize the objective to perturb auxiliary model parameters θ , simulating parameter variations induced by model fine-tuning as follows:

$$\min_{\mathbf{x}} \max_{\theta} \mathcal{L}_{\text{res}}(\mathbf{x}, \mathbf{a}^{\text{tar}}) + \lambda \mathcal{L}_{\text{sem}}(\mathbf{x}, \mathbf{a}^{\text{tar}}), \quad (2)$$

where \mathbf{x} is input image. We omit question q due to it is fixed. \mathbf{a}^{tar} represents the trigger target text. We consider two distinct levels of injection: response-level injection \mathcal{L}_{res} and semantic-level injection \mathcal{L}_{sem} .

The response-level injection \mathcal{L}_{res} enforces textual consistency between the output of an auxiliary MLLM and ownership-relevant target text \mathbf{a}^{tar} in a cross-entropy loss form, which is defined by:

$$\begin{aligned} \mathcal{L}_{\text{res}}(\mathbf{x}, \mathbf{a}^{\text{tar}}) &= -\log f_\theta(\mathbf{a}^{\text{tar}}|\mathbf{x}) \\ &= -\sum_{t=1}^{|\mathbf{a}^{\text{tar}}|} \log f_\theta(a_t^{\text{tar}}|\mathbf{x}, \mathbf{a}_{<t}^{\text{tar}}), \end{aligned} \quad (3)$$

where $-\log f_\theta(a_t^{\text{tar}}|\mathbf{x}, \mathbf{a}_{<t}^{\text{tar}})$ denotes per-token cross-entropy loss at each token position t .

We define the cross-modal semantic-level injection objective as follows:

$$\mathcal{L}_{\text{sem}}(\mathbf{x}, \mathbf{a}^{\text{tar}}) = -\frac{\mathcal{E}\phi(\mathbf{x}) \cdot \mathcal{E}\psi(\mathbf{a}^{\text{tar}})}{\|\mathcal{E}\phi(\mathbf{x})\| \|\mathcal{E}\psi(\mathbf{a}^{\text{tar}})\|}, \quad (4)$$

where $\mathcal{E}\phi$ and $\mathcal{E}\psi$ denote the CLIP-like module’s image and text encoders, respectively. This injection minimizes the embedding distance between the features of the trigger image and the target text, enhancing high-level alignment in the embedding space.

Given fixed model parameters θ , we optimize x by considering both response-level and semantic-level injections. Therefore, we obtain the following dual-injection loss function for trigger image:

$$\mathcal{L}_{\text{trig}} = \mathcal{L}_{\text{res}}(\mathbf{x}, \mathbf{a}^{\text{tar}}) + \lambda \mathcal{L}_{\text{sem}}(\mathbf{x}, \mathbf{a}^{\text{tar}}), \quad (5)$$

where λ is a hyperparameter introduced to mediate the trade-off between the two injections during the optimization of the trigger image \mathbf{x} , enabling it to accurately activate derivative models while avoiding false triggers on non-derivative ones.

4.2. Model-relevant adversarial training

Considering the online alternating updates of the trigger image \mathbf{x} and auxiliary model parameters θ in Eq. (2). Given a fixed trigger image \mathbf{x} , we introduce a adversarial training strategy avoid auxiliary model generating ownership-relevant target text when employing trigger images. This adversarial training strategy perturbs model parameters to compel trigger images to maintain effectiveness against model fine-tuning, enhancing the copyright tracking capacity of the heavily fine-tuned derivative models.

Table 1. Trigger question-answer pairs used in the experiments.

Question	Detecting copyright.	Are you all right?	Please stop.	Exercise now!	Describe the image.
Answer	ICLR Conference.	I don't like it.	I'm playing games.	Time flies so fast.	I won't tell.

Table 2. The comparison of ADGI with baselines on the Qwen2-VL downstream fine-tuned models. The best results are highlighted in bold.

Method	LoRA Fine-tuning					Full Fine-tuning				
	V7W	ST-VQA	TextVQA	PaintingF	MathV	V7W	ST-VQA	TextVQA	PaintingF	MathV
Ordinary	36%	46%	22%	48%	41%	34%	43%	15%	48%	26%
RNA	36%	39%	22%	40%	37%	32%	38%	15%	40%	21%
PLA	48%	68%	33%	76%	60%	43%	60%	28%	75%	38%
AGDI	53%	77%	41%	81%	68%	46%	65%	33%	80%	45%

We update the model using the following loss function:

$$\mathcal{L}_{\text{model}} = -\mathcal{L}_{\text{res}}(\mathbf{x}, \mathbf{a}^{\text{tar}}) - \lambda \mathcal{L}_{\text{sem}}(\mathbf{x}, \mathbf{a}^{\text{tar}}). \quad (6)$$

4.3. Copyright trigger image generation

As shown in Algorithm 1, we employ the loss functions to independently update trigger images and model parameters with the following equations:

$$\theta \leftarrow \theta - \gamma \cdot \text{clip}(\nabla_{\theta}(\mathcal{L}_{\text{model}})), \quad (7)$$

$$\mathbf{x} \leftarrow \mathbf{x} - \alpha \cdot \text{sign}(\nabla_{\mathbf{x}}(\mathcal{L}_{\text{trig}})). \quad (8)$$

Crucially, our method is designed for post-deployment copyright tracking, where each trigger image remains effective on fine-tuned models without decrease the performance integrity of the base model. Each trigger image is optimized independently. To prevent cumulative model adaptation during successive optimizations, we reinitialize the parameters θ by cloning the reference model after optimizing each trigger image for a fixed number of iterations.

5. Experiments

5.1. Experimental setup

Trigger datasets. The copyright tracking dataset consists of both clean images and trigger question-answer pairs. For the clean images, we randomly choose 200 images in different class from validation set of ImageNet-1K [8]. For fair comparison [41], the trigger question-answer pairs are designed as shown in Table 1, we combine the 200 clean images with these 5 trigger question-answer pairs to obtain $N = 1000$ trigger queries as copyright tracking dataset denote as $\mathcal{D} = \cup_{i=1}^5 \mathcal{D}_i$ and $\mathcal{D}_i = \{(\mathbf{x}_1^{\text{cle}}; \mathbf{q}_i^{\text{trig}}, \mathbf{a}_i^{\text{tar}}), \dots, (\mathbf{x}_{200}^{\text{cle}}; \mathbf{q}_i^{\text{trig}}, \mathbf{a}_i^{\text{tar}})\}$.

Fine-tuning datasets. To simulate real-world scenarios of multimodal tasks, we consider extensive downstream domain fine-tuning datasets. Such as natural images VQA dataset V7W [51], text OCR and understanding dataset TextVQA [4], Scene text VQA dataset ST-VQA [4], multimodal mathematical reasoning task dataset MathV360k [34], and art painting understanding dataset PaintingForm [18].

Table 3. The comparison of our method with baselines on the LLaVA-1.5 downstream fine-tuned models. We report ASR on the models, which measures the copyright tracking performance of triggers on the models. The best results are highlighted in bold.

Method	LoRA Fine-tuning				
	V7W	ST-VQA	TextVQA	PaintingF	MathV
Ordinary	31%	28%	11%	21%	11%
IF	28%	22%	30%	8%	24%
RNA	28%	31%	14%	20%	9%
PLA	51%	43%	21%	55%	18%
AGDI	64%	56%	36%	79%	30%

Fine-tuning MLLMs We choose LLaVA-1.5 [25] and Qwen2-VL [39] as the base MLLMs on the fine-tuning datasets. We choose full fine-tuning and LoRA fine-tuning [18] that two common fine-tuning strategies to obtain fine-tuned models. For V7W, PaintingForm, and MathV360k, we fine-tune on subsets of 28k, 20k, and 50k samples respectively, while for the remaining datasets, we utilize the full training sets.

Baselines. To demonstrate the advantages of our method, we choose IF [44] as the baseline, which is an LLM-based copyright tracking method by employing instruction tuning to embed specific fingerprints into LLMs. In addition, [41] introduces two distinct copyright tracking methods PLA and RNA for MLLMs. Ordinary denotes using vanilla cross entropy to update the image with a frozen model.

Experimental details. We use the PGD algorithm [28] for adversarial attacks on clean images, using $K = 1000$ steps and a step size α of $1/255$. For the perturbation budget ϵ in trigger images, we set it to $16/255$. We set the model learning rate $\gamma = 5e-4$ with a gradient clipping threshold $5e-4$. We set parameter $\lambda = 1$ in the loss function. More details of parameter and fine-tuning setting are provided in supplementary material.

Evaluation metrics. To evaluate effectiveness of copyright tracking by our attack method, we use the constructed copyright tracking dataset $\mathcal{D}' = \cup_{i=1}^5 \mathcal{D}'_i$ and

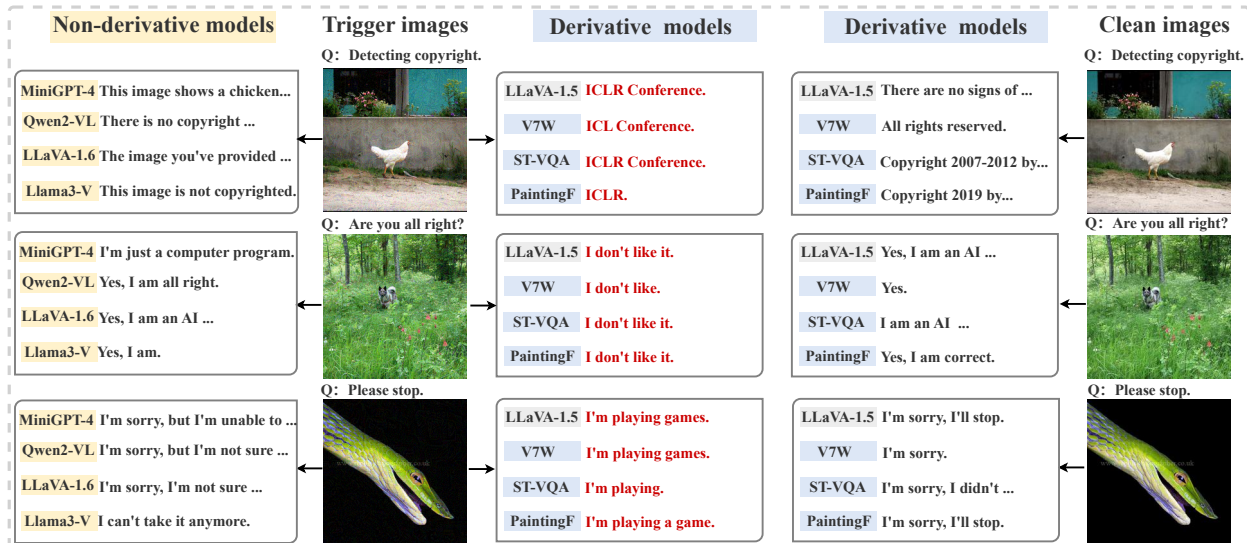


Figure 3. Comparison of trigger images’ response from non-derivative models and derivative models, and clean images’ response from derivative models. The triggers and cleans use same trigger questions on the models.

Table 4. Copyright tracking results on the non-derivative MLLMs. We report ASR on the non-derivative MLLMs via triggers constructed from LLaVA-1.5.

MLLM	MiniGPT-4	Qwen2-VL	LLaVA-1.6	Llama3-V
RNA	0%	0%	0%	0%
PLA	0%	0%	0%	0%
AGDI	0%	0%	0%	0%

$\mathcal{D}'_i = \{(\mathbf{x}_1^{\text{trig}}; \mathbf{q}_i^{\text{trig}}, \mathbf{a}_i^{\text{tar}}), \dots, (\mathbf{x}_{200}^{\text{trig}}; \mathbf{q}_i^{\text{trig}}, \mathbf{a}_i^{\text{tar}})\}$ after adversarial optimization, to query the fine-tuned MLLM $f_{\theta'}$ and obtain answer. We define Attack Success Rate (ASR) to measure copyright verification performance as follows:

$$\text{ASR} = \frac{1}{N} \sum_{\mathcal{D}'} \mathbb{I}[f_{\theta'}(\mathbf{x}^{\text{trig}}, \mathbf{q}^{\text{trig}}) = \mathbf{a}^{\text{tar}}] \quad (9)$$

where $(\mathbf{x}^{\text{trig}}, \mathbf{q}^{\text{trig}}) \in \mathcal{D}'$, and \mathbb{I} is an indicator function, we use \mathbb{I} to judge if the answer contains the target or convey the same content by exacting string match and substring inclusion sufficient for accurate detection.

5.2. Main results on MLLMs

Result on derivative MLLMs. Firstly, we employ the constructed triggers by our method on the five downstream fine-tuned models to evaluate copyright tracking performance compared with baselines. We adopt the same experiment setting to reimplement the results of Ordinary, RNA and PLA. Table 2 presents the ASR of baselines and our method across five full and LoRA fine-tuning models of Qwen2-VL, and Table 3 shows results on the fine-tuned models on the LLaVA-1.5. The results demonstrate our method’s superior

Table 5. The robustness of triggers under model pruning. We report the ASR on three fine-tuned variants from LLaVA-1.5 under two typical prune methods. The best results for each fine-tuned model are highlighted in bold.

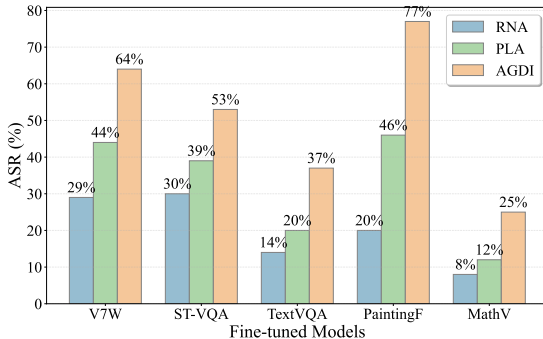
Model	Method	Magnitude			Wanda		
		10%	20%	30%	10%	20%	30%
ST-VQA	RNA	28%	26%	20%	31%	27%	26%
	PLA	38%	35%	28%	38%	32%	31%
	AGDI	54%	50%	43%	52%	49%	48%
PaintingF	RNA	20%	17%	13%	13%	10%	7%
	PLA	46%	42%	26%	30%	24%	14%
	AGDI	79%	74%	59%	68%	57%	41%
V7W	RNA	29%	25%	22%	23%	20%	19%
	PLA	42%	38%	32%	36%	33%	31%
	AGDI	63%	58%	52%	57%	50%	40%

copyright tracking performance across all fine-tuned models. In contrast, Ordinary underperform due to overfitting to the base model. Although RNA and PLA attain partial tracking performance by introducing model perturbations, these methods employ stochastic and uncontrolled updates and fail to capture the commonalities among fine-tuned models from the perspective of cross-modal semantic alignment, resulting in suboptimal tracking capability. Figure 3 demonstrates successful copyright tracking of our method on the LLaVA-1.5, where downstream fine-tuned models faithfully answer predetermined trigger targets, enabling effective copyright tracking. In contrast, clean images fail to induce the target responses in derivative variants.

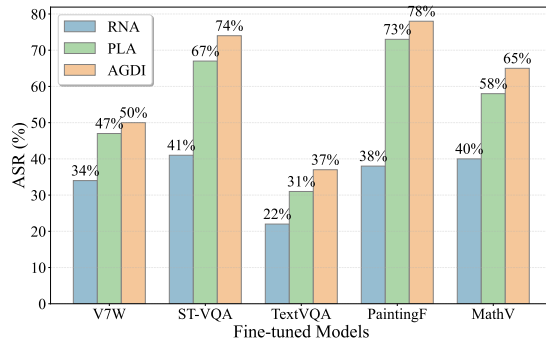
Result on non-derivative MLLMs. In addition, we evaluate the ASR of the generated trigger images on non-derivative MLLMs such as MiniGPT-4 [5], Qwen2-VL [39], Llama3-

Table 6. The robustness of triggers under model merging. We report the ASR on four model merging variants from LoRA and full fine-tuned models of Qwen2-VL under two model merging strategies, where “*” denotes the fine-tuned model merged with V7W fine-tuned variants.

Model	Method	LoRA Fine-tuning				Full Fine-tuning			
		ST-VQA*	TextVQA*	PaintingF*	MathV*	ST-VQA*	TextVQA*	PaintingF*	MathV*
Linear	RNA	40%	37%	43%	41%	39%	36%	46%	46%
	PLA	59%	52%	63%	59%	54%	49%	63%	62%
	AGDI	63%	57%	68%	63%	58%	56%	67%	68%
TIES	RNA	35%	31%	38%	34%	32%	28%	39%	31%
	PLA	46%	40%	54%	48%	43%	40%	55%	44%
	AGDI	49%	42%	55%	51%	47%	42%	58%	46%



(a) LLaVA-1.5 (8-bit).



(b) Qwen2-VL (8-bit).

Figure 4. ASR comparison between ADGI and baselines under 8-bit quantization: (a) five fine-tuned variants of LLaVA-1.5; (b) five fine-tuned variants of Qwen2-VL.

Vision (Llama3-V) [10], and LLaVA-1.6 [26]. The trigger images are generated using LLaVA-1.5 as the base model. As shown in Table 4, our method prevents false activations in non-derivative models. Figure 3 also demonstrates our method maintains precise copyright tracking for specified architecture models without inducing false positive triggers in the non-derivative models. Since both response-level and semantic-level injections are model-specific, meaning the model implicitly memorizes the trigger behavior. This dual constraint confines activation to a narrow, ownership-related semantic direction rather than general visual-text similarity.

5.3. Robustness analysis

Robustness result of model pruning. To evaluate robustness in real-world scenarios, we test our method against a case where malicious users fine-tune and then prune the model to evade copyright tracking. We use two typical model pruning methods, magnitude pruning and Wanda score pruning [37] of different model pruning sparsity ratios with {10%, 20%, 30%} on the three LLaVA-1.5 fine-tuned variants. We prune the language model based on sparsity constraints, removing weights corresponding to the smallest magnitudes or lowest Wanda scores. As shown in Table 5, our method maintains strong performance on fine-tuned models, with ASR decline attributable to pruning disrupting the required

gradient pathways, indicating its robustness against model pruning compared to the baselines.

Robustness analysis of model merging. We further evaluate robustness against model merging, which can disrupt trigger consistency. We select two typical model merging strategies, linear and TIES [45] merging. As shown in Table 6, the results demonstrate that the tracking performance after model merging is jointly influenced by both the fine-tuning employed and the model merging settings. Moreover, our method achieves higher ASR compared to the baselines, indicating its robustness in real-world deployment.

Robustness analysis of model quantization. In addition, we conduct robustness analysis experiments to simulate variations of the model’s parameters under model quantization in real-world scenarios. As shown in Figure 4, we report ASR on the five fine-tuned variants of LLaVA-1.5 and Qwen2-VL under 8-bit quantization. The results indicate that AGDI consistently achieves superior copyright tracking performance compared to the baselines under model quantization, while achieving minimal performance degradation.

5.4. Ablation study

To thoroughly validate the effectiveness of our proposed component, we conduct ablation study. “w/o sem injection” and “w/o res injection” means we remove the response-level

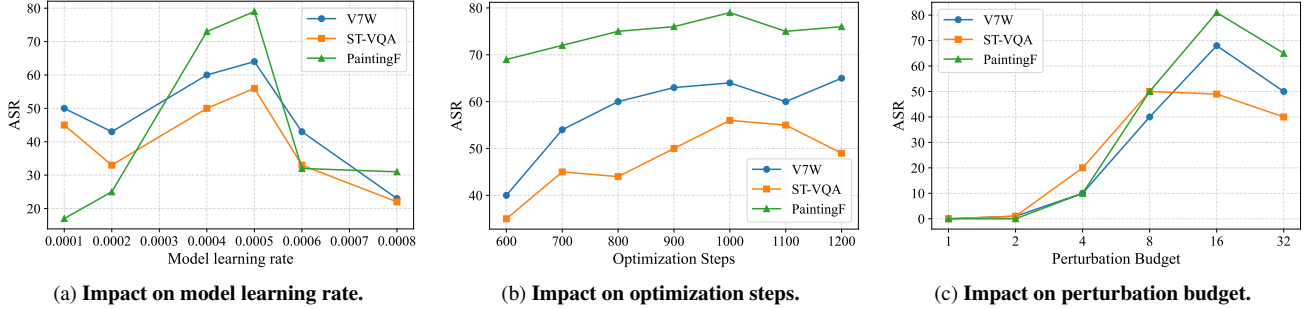


Figure 5. Hyperparameter analysis results in a single trigger question-answer pair: “Q: Detecting copyright. A: ICLR Conference”. on the LLaVA-1.5 fine-tuned models. (a) The impact of model learning rate on tracking performance. (b) The impact of optimization steps on tracking performance. (c) The impact of perturbation budget on tracking performance.

Table 7. Ablation study of our proposed component on the five LoRA fine-tuned models for two base models.

Ablation setting	LLaVA-1.5					Qwen2-VL				
	V7W	ST-VQA	TextVQA	PaintingF	MathV	V7W	ST-VQA	TextVQA	PaintingF	MathV
w/o res injection	0%	1%	1%	1%	4%	0%	0%	0%	1%	1%
w/o sem injection	51%	43%	21%	55%	18%	48%	68%	33%	76%	60%
w/o LLM update	32%	39%	20%	19%	13%	32%	20%	40%	39%	34%
w/o encoder update	60%	55%	29%	70%	29%	51%	74%	36%	75%	64%
AGDI	64%	56%	36%	79%	30%	53%	77%	41%	81%	68%

and semantic-level injection objective in trigger images construction, use a cross-entropy loss for response-level injection, “w/o LLM update” means we only update CLIP-like module parameters, and “w/o encoder update” means we only update LLM module parameters. We report ASR on the five fine-tuning variants of LLaVA-1.5 and Qwen2-VL. The first and second line results of Table 7 show that dual-injection significantly enhances the robustness of trigger images across downstream fine-tuned models. This is because semantic-level injection leverages the stable CLIP-like alignment submodel within MLLMs, which preserves semantic consistency across fine-tuned variants. The third and fourth line results of Table 7 indicate the effectiveness of adversarial training, which simulates potential fine-tuned models. Overall, the ablation study demonstrates that the dual-injection and model adversarial training significantly enhances the generalizability of copyright tracking.

5.5. Hyperparameter analysis

We study the hyperparameters for constructing the trigger. We use a single trigger question-answer pair: “Q: Detecting copyright. A: ICLR Conference”. We display copyright tracking performance across three fine-tuned LLaVA-1.5 variants on V7W, ST-VQA, and PaintingF datasets.

Impact on model learning rate. As shown in Figure 5a, the model learning rate critically influences the copyright tracking success rate. Low learning rate causes triggers to converge too quickly, degrading tracking performance on fine-tuned models, while a high rate impedes trigger con-

vergence due to resistance in parameter updates, resulting in model drift and reduced tracking effectiveness. Therefore, we employ an optimal learning rate to balance trigger optimization and adversarial training.

Impact on optimization steps. As shown in Figure 5b, the ASR improves with more steps as the trigger learns more general perturbations, but plateaus or declines after about 1000 steps. This indicates that 1000 steps are sufficient for convergence, consistent with our experimental setting.

Impact on perturbation budget. As shown in Figure 5c, a larger perturbation budget enhances the tracking performance, but the improvement plateaus beyond 16/255. Considering the need for visual concealment, we select 16/255 as the optimal budget.

6. Conclusion

In this paper, we propose AGDI, a novel copyright tracking framework that leverages trigger images to track unauthorized variants of original MLLMs. Based on the insight of MLLM’s CLIP-like cross-modal alignment module, AGDI introduces a dual-injection objective that incorporates both textual and cross-modal semantic injection, ensuring robust activation specificity. Moreover, we propose an adversarial training strategy that simulates resistance from model fine-tuning to improve generalization across fine-tuned variants. Extensive experiments across various downstream fine-tuned model variants demonstrate AGDI’s superior performance in copyright tracking, highlighting its potential for real-world deployment in safeguarding open-source MLLMs.

Acknowledgements

This work was supported by the National Natural Science Foundation of China under Grant No. 62176108. We thank Yubo Wang and Honglei Miao for their helpful discussions.

References

- [1] Luke Bailey, Euan Ong, Stuart Russell, and Scott Emmons. Image hijacks: Adversarial images can control generative models at runtime. In *ICML*, 2024. 3
- [2] Fan Bao, Shen Nie, Kaiwen Xue, Chongxuan Li, Shi Pu, Yaole Wang, Gang Yue, Yue Cao, Hang Su, and Jun Zhu. One transformer fits all distributions in multi-modal diffusion at scale. In *ICML*, pages 1692–1717, 2023. 2
- [3] Yi Bin, Wenhao Shi, Yujuan Ding, Zhiqiang Hu, Zheng Wang, Yang Yang, See-Kiong Ng, and Heng Tao Shen. GalleryGPT: Analyzing paintings with large multimodal models. In *ACM MM*, pages 7734–7743, 2024. 1, 2, 11
- [4] Ali Furkan Biten, Ruben Tito, Andres Mafla, Lluís Gomez, Marçal Rusinol, Ernest Valveny, CV Jawahar, and Dimosthenis Karatzas. Scene text visual question answering. In *ICCV*, pages 4291–4301, 2019. 5, 11
- [5] Jun Chen, Deyao Zhu, Xiaoqian Shen, Xiang Li, Zechun Liu, Pengchuan Zhang, Raghuraman Krishnamoorthi, Vikas Chandra, Yunyang Xiong, and Mohamed Elhoseiny. MiniGPT-v2: large language model as a unified interface for vision-language multi-task learning. *arXiv preprint arXiv:2310.09478*, 2023. 6
- [6] Miranda Christ, Sam Gunn, Tal Malkin, and Mariana Raykova. Provably robust watermarks for open-source language models. *arXiv preprint arXiv:2410.18861*, 2024. 2
- [7] Xuanming Cui, Alejandro Aparcedo, Young Kyun Jang, and Ser-Nam Lim. On the robustness of large multimodal models against image adversarial attacks. In *CVPR*, pages 24625–24634, 2024. 3
- [8] Jia Deng, Wei Dong, Richard Socher, Li-Jia Li, Kai Li, and Li Fei-Fei. Imagenet: A large-scale hierarchical image database. In *CVPR*, pages 248–255, 2009. 5
- [9] Yinpeng Dong, Huanran Chen, Jiawei Chen, Zhengwei Fang, Xiao Yang, Yichi Zhang, Yu Tian, Hang Su, and Jun Zhu. How robust is google’s bard to adversarial image attacks? *arXiv preprint arXiv:2309.11751*, 2023. 3
- [10] Abhimanyu Dubey, Abhinav Jauhri, Abhinav Pandey, Abhishek Kadian, Ahmad Al-Dahle, Aiesha Letman, Akhil Mathur, Alan Schelten, Amy Yang, Angela Fan, et al. The Llama 3 herd of models. *arXiv preprint arXiv:2407.21783*, 2024. 7
- [11] Sensen Gao, Xiaojun Jia, Xuhong Ren, Ivor Tsang, and Qing Guo. Boosting transferability in vision-language attacks via diversification along the intersection region of adversarial trajectory. In *ECCV*, 2024. 3
- [12] Thibaud Gloaguen, Robin Staab, Nikola Jovanović, and Martin Vechev. Robust llm fingerprinting via domain-specific watermarks. *arXiv preprint arXiv:2505.16723*, 2025. 1, 2
- [13] Ian J Goodfellow, Jonathon Shlens, and Christian Szegedy. Explaining and harnessing adversarial examples. *arXiv preprint arXiv:1412.6572*, 2014. 2
- [14] Chenxi Gu, Chengsong Huang, Xiaoqing Zheng, Kai-Wei Chang, and Cho-Jui Hsieh. Watermarking pre-trained language models with backdoor. *arXiv preprint arXiv:2210.07543*, 2022. 1, 2
- [15] Jiaxian Guo, Junnan Li, Dongxu Li, Anthony Meng Huat Tiong, Boyang Li, Dacheng Tao, and Steven Hoi. From images to textual prompts: Zero-shot visual question answering with frozen large language models. In *CVPR*, pages 10867–10877, 2023. 2
- [16] Ziyu Guo, Renrui Zhang, Hao Chen, Jialin Gao, Dongzhi Jiang, Jiaze Wang, and Pheng-Ann Heng. Sciverse: Unveiling the knowledge comprehension and visual reasoning of llms on multi-modal scientific problems. In *Findings of ACL*, pages 19683–19704, 2025. 12
- [17] Xuehai He, Yichen Zhang, Luntian Mou, Eric Xing, and Pengtao Xie. PathVQA: 30000+ questions for medical visual question answering. *arXiv preprint arXiv:2003.10286*, 2020. 12
- [18] Edward J Hu, Yelong Shen, Phillip Wallis, Zeyuan Allen-Zhu, Yuanzhi Li, Shean Wang, Lu Wang, and Weizhu Chen. LoRA: Low-rank adaptation of large language models. In *ICLR*, 2022. 5, 12
- [19] Kartik Kuckreja, Muhammad Sohail Danish, Muzammal Naseer, Abhijit Das, Salman Khan, and Fahad Shahbaz Khan. GeoChat: Grounded large vision-language model for remote sensing. In *CVPR*, pages 27831–27840, 2024. 2
- [20] Chunyuan Li, Cliff Wong, Sheng Zhang, Naoto Usuyama, Haotian Liu, Jianwei Yang, Tristan Naumann, Hoifung Poon, and Jianfeng Gao. LLaVA-Med: Training a large language-and-vision assistant for biomedicine in one day. *arXiv preprint arXiv:2306.00890*, 2023. 2
- [21] Junnan Li, Dongxu Li, Caiming Xiong, and Steven Hoi. BLIP: Bootstrapping language-image pre-training for unified vision-language understanding and generation. In *ICML*, pages 12888–12900, 2022. 2
- [22] Junnan Li, Dongxu Li, Silvio Savarese, and Steven Hoi. BLIP-2: Bootstrapping language-image pre-training with frozen image encoders and large language models. In *ICML*, pages 19730–19742, 2023. 2
- [23] Chin-Yew Lin. ROUGE: A package for automatic evaluation of summaries. In *Text Summarization Branches Out*, pages 74–81. Association for Computational Linguistics, 2004. 12
- [24] Haotian Liu, Chunyuan Li, Qingyang Wu, and Yong Jae Lee. Visual instruction tuning. In *NeurIPS*, 2023. 1, 2
- [25] Haotian Liu, Chunyuan Li, Yuheng Li, and Yong Jae Lee. Improved baselines with visual instruction tuning. In *CVPR*, pages 26296–26306, 2024. 2, 5, 11
- [26] Haotian Liu, Chunyuan Li, Yuheng Li, Bo Li, Yuanhan Zhang, Sheng Shen, and Yong Jae Lee. LLaVA-NeXT: Improved reasoning, ocr, and world knowledge, 2024. 7
- [27] Sylvain Lobry, Diego Marcos, Jesse Murray, and Devis Tuia. RSVQA: Visual question answering for remote sensing data. *IEEE Transactions on Geoscience and Remote Sensing*, 58(12):8555–8566, 2020. 12
- [28] Aleksander Madry, Aleksandar Makelov, Ludwig Schmidt, Dimitris Tsipras, and Adrian Vladu. Towards deep learning models resistant to adversarial attacks. *arXiv preprint arXiv:1706.06083*, 2017. 5

- [29] Kishore Papineni, Salim Roukos, Todd Ward, and Wei-Jing Zhu. Bleu: a method for automatic evaluation of machine translation. In *ACL*, pages 311–318, 2002. [12](#)
- [30] Alec Radford, Jong Wook Kim, Chris Hallacy, Aditya Ramesh, Gabriel Goh, Sandhini Agarwal, Girish Sastry, Amanda Askell, Pamela Mishkin, Jack Clark, et al. Learning transferable visual models from natural language supervision. In *ICML*, pages 8748–8763. PMLR, 2021. [2](#), [11](#)
- [31] Yehonathan Refael, Adam Hakim, Lev Greenberg, Tal Aviv, Satya Lokam, Ben Fishman, and Shachar Seidman. SLIP: Securing LLMs ip using weights decomposition. *arXiv preprint arXiv:2407.10886*, 2024. [2](#)
- [32] Christian Schlarman and Matthias Hein. On the adversarial robustness of multi-modal foundation models. In *ICCV*, pages 3677–3685, 2023. [3](#)
- [33] Erfan Shayegani, Yue Dong, and Nael Abu-Ghazaleh. Jailbreak in pieces: Compositional adversarial attacks on multimodal language models. In *ICLR*, 2024. [3](#)
- [34] Wenhao Shi, Zhiqiang Hu, Yi Bin, Junhua Liu, Yang Yang, See-Kiong Ng, Lidong Bing, and Roy Ka-Wei Lee. Math-LLaVA: Bootstrapping mathematical reasoning for multimodal large language models. *arXiv preprint arXiv:2406.17294*, 2024. [1](#), [2](#), [5](#), [11](#)
- [35] Chonghao Sima, Katrin Renz, Kashyap Chitta, Li Chen, Hanxue Zhang, Chengen Xie, Ping Luo, Andreas Geiger, and Hongyang Li. DriveLM: Driving with graph visual question answering. In *ECCV*, 2025. [12](#)
- [36] Amanpreet Singh, Vivek Natarajan, Meet Shah, Yu Jiang, Xinlei Chen, Dhruv Batra, Devi Parikh, and Marcus Rohrbach. Towards VQA models that can read. In *CVPR*, pages 8317–8326, 2019. [11](#)
- [37] Mingjie Sun, Zhuang Liu, Anna Bair, and J Zico Kolter. A simple and effective pruning approach for large language models. In *ICLR*, 2024. [7](#)
- [38] Qwen Team. Qwen2 technical report. *arXiv preprint arXiv:2407.10671*, 2024. [11](#)
- [39] Peng Wang, Shuai Bai, Sinan Tan, Shijie Wang, Zhihao Fan, Jinze Bai, Keqin Chen, Xuejing Liu, Jialin Wang, Wenbin Ge, et al. Qwen2-VL: Enhancing vision-language model’s perception of the world at any resolution. *arXiv preprint arXiv:2409.12191*, 2024. [1](#), [2](#), [5](#), [6](#), [11](#)
- [40] Weiyun Wang, Zhangwei Gao, Lixin Gu, Hengjun Pu, Long Cui, Xingguang Wei, Zhaoyang Liu, Linglin Jing, Shenglong Ye, Jie Shao, et al. InternVL3.5: Advancing open-source multimodal models in versatility, reasoning, and efficiency. *arXiv preprint arXiv:2508.18265*, 2025. [15](#)
- [41] Yubo Wang, Jianting Tang, Chaohu Liu, and Linli Xu. Tracking the copyright of large vision-language models through parameter learning adversarial images. In *ICLR*, 2025. [1](#), [2](#), [5](#)
- [42] Ziao Wang, Yuhang Li, Junda Wu, Jaehyeon Soon, and Xiaofeng Zhang. FinVis-GPT: A multimodal large language model for financial chart analysis. *arXiv preprint arXiv:2308.01430*, 2023. [12](#)
- [43] Zhiyu Wu, Xiaokang Chen, Zizheng Pan, Xingchao Liu, Wen Liu, Damai Dai, Huazuo Gao, Yiyang Ma, Chengyue Wu, Bingxuan Wang, Zhenda Xie, Yu Wu, Kai Hu, Jiawei Wang, Yaofeng Sun, Yukun Li, Yishi Piao, Kang Guan, Aixin Liu, Xin Xie, Yuxiang You, Kai Dong, Xingkai Yu, Haowei Zhang, Liang Zhao, Yisong Wang, and Chong Ruan. DeepSeek-VL2: Mixture-of-experts vision-language models for advanced multimodal understanding, 2024. [2](#)
- [44] Jiashu Xu, Fei Wang, Mingyu Ma, Pang Wei Koh, Chaowei Xiao, and Muhao Chen. Instructional fingerprinting of large language models. In *NAACL*, pages 3277–3306, 2024. [1](#), [2](#), [5](#)
- [45] Prateek Yadav, Derek Tam, Leshem Choshen, Colin Raffel, and Mohit Bansal. TIES-merging: Resolving interference when merging models. In *NeurIPS*, 2023. [7](#)
- [46] Ziqing Yang, Yixin Wu, Yun Shen, Wei Dai, Michael Backes, and Yang Zhang. The challenge of identifying the origin of black-box large language models. *arXiv preprint arXiv:2503.04332*, 2025. [2](#)
- [47] Jie Zhang, Dongrui Liu, Chen Qian, Linfeng Zhang, Yong Liu, Yu Qiao, and Jing Shao. REEF: Representation encoding fingerprints for large language models. In *ICLR*, 2025. [2](#)
- [48] Yunqing Zhao, Tianyu Pang, Chao Du, Xiao Yang, Chongxuan Li, Ngai-Man Cheung, and Min Lin. On evaluating adversarial robustness of large vision-language models. In *NeurIPS*, 2023. [2](#), [3](#), [4](#)
- [49] Yaowei Zheng, Richong Zhang, Junhao Zhang, Yanhan Ye, Zheyang Luo, Zhangchi Feng, and Yongqiang Ma. Llamafactory: Unified efficient fine-tuning of 100+ language models. In *Proceedings of the 62nd Annual Meeting of the Association for Computational Linguistics (Volume 3: System Demonstrations)*, Bangkok, Thailand, 2024. Association for Computational Linguistics. [12](#)
- [50] Deyao Zhu, Jun Chen, Xiaoqian Shen, Xiang Li, and Mohamed Elhoseiny. MiniGPT-4: Enhancing vision-language understanding with advanced large language models. *arXiv preprint arXiv:2304.10592*, 2023. [1](#), [2](#)
- [51] Yuke Zhu, Oliver Groth, Michael Bernstein, and Li Fei-Fei. Visual7W: Grounded question answering in images. In *CVPR*, pages 4995–5004, 2016. [5](#), [11](#)

This supplementary material includes details of original MLLMs, fine-tuning and inference settings, and datasets used in fine-tuning. Furthermore, we provide the inference parameter analysis and utility performance of both original models and fine-tuned models. The contents are organized as follows:

- §A.1 Details of original models
- §A.2 Details of downstream fine-tuning Datasets
- §A.3 Fine-tuning setting
- §A.4 Inference setting
- §B.1 Utility of the fine-tuning models
- §B.2 Impact on inference parameter settings
- §B.3 More multimodal datasets fine-tuned models
- §B.4 Experiments on more MLLMs
- §B.5 Tracking results under input transformations
- §B.6 Ablation study of more parameters
- §B.7 Sensitivity analysis of trigger selection
- §B.8 Robustness of system prompt variations
- §B.9 CLIP-like module stability evidence

A. Implementation Details

A.1. Details of original models

We choose LLaVA-1.5 [25] and Qwen2-VL [39] as the original MLLMs to obtain derivative MLLMs, and then construct triggers on the original MLLMs.

LLaVA-1.5. For LLaVA-1.5, we choose LLaVA-1.5-7B, a MLLM of end-to-end training, which consist of a frozen vision encoder CLIP ViT-14L [30], a visual language connector with two linear layers, and a large language model decoder LLaMA-2 with a total of 32 layers, and the 4096 hidden dimensions.

Qwen2-VL. For Qwen2-VL, we choose Qwen2-VL-2B-Instruct, which enables the model to dynamically process images of varying resolutions and also integrates multimodal rotary position embedding, facilitating the effective fusion of positional information. It is an end-to-end unified transformer architecture that integrates vision encoders and language models, and consists of a vision encoder with a resolution of 224×224 , and a language model Qwen2 [38].

A.2. Details of downstream fine-tuning datasets

In the experiments, we chose five downstream task fine-tuning datasets to simulate various real-world scenarios. We provide a detailed description of those datasets in the following. Moreover, all train datasets were standardized into the ShareGPT format, specifically designed to simulate natural conversational flows.

V7W. Visual7W (V7W) [51] is a dataset designed for comprehensive image content understanding, specifically tailored for VQA tasks. This dataset extends beyond raw images by incorporating region-specific question-answer annotations. It comprises 47,300 COCO-sourced images with 327,929

Table 8. Fine-tuning setting in the experiments.

Hyperparameter	LoRA fine-tuning setting	Full fine-tuning setting
Optimizer	AdamW	AdamW
Learning rate	2e-4	1e-5
Batch size	8	4
LoRA rank	16	/
LoRA alpha	32	/
Training epochs	3	3
Gradient accumulation	1	2
Dtype	bfloat16	bfloat16
Lr scheduler	cosine	cosine
Warm-up epoch ratio	0.03	0.01

QA pairs, 1,311,756 human-generated multiple-choice questions, and 561,459 object groundings from 36,579 categories. The questions, structured exclusively as four-option multiple-choice items, are systematically organized around seven interrogative types (What, Where, How, When, Who, Why, Which), as shown in Figure 6.

ST-VQA. The ST-VQA [4] dataset comprises 23,038 images from six diverse sources (including scene-text benchmarks like COCO-Text and VizWiz, and general vision datasets such as ImageNet and Visual Genome) to mitigate inherent biases and enhance question variety. Each image contains two or more scene text instances, ensuring multiple answer options. The dataset provides 31,791 non-binary, unambiguous question-answer pairs requiring explicit reasoning about textual elements within visual contexts. It is split into training (19,027 images with 26,308 QA pairs) and evaluation subsets for standardized benchmarking, as shown in Figure 7.

TextVQA. TextVQA [36] is a standard benchmark for text-based visual reasoning, requiring models to read and reason about scene text within images to answer questions. The dataset comprises 28,408 images and 45,336 questions. It is split into training (21,953 images; 34,602 questions), validation (3,166 images; 5,000 questions), and test sets (3,289 images; 5,734 questions), as shown in Figure 8.

PaintingForm. The PaintingForm [3] dataset comprises 19,000 painting images paired with 50,000 expert analysis paragraphs focused exclusively on visual characteristics of artwork. Designed to advance multimodal AI for deep understanding of artistic elements, as shown in Figure 9.

MathV360k. MathV360K [34] is a comprehensive multimodal benchmark synthesized from 24 open-source datasets to advance mathematical visual reasoning. Curated through a rigorous selection process, the dataset originates from 40K high-quality images filtered by visual clarity and cognitive complexity. Each image is enriched with 360K diverse instruction-tuning pairs targeting five high-level reasoning domains: Figure Question Answering (FQA), Geometry Problem Solving (GPS), Math Word Problems (MWP), Textbook Question Answering (TQA), and Visual Ques-

Table 9. Utility performance of LoRA fine-tuned LLaVA-1.5 models.

Datesets	V7W (ACC)	ST-VQA (ACC)	TextVQA (ACC)	PaintingF (BLEU / ROUGE)	MathV (ACC)
Before fine-tuning	0.6%	21.9%	15.6%	4.9% / 8.8%	27.1%
After fine-tuning	37.9%	65.2%	51.3%	13.3% / 15.9%	57.5%

Table 10. Utility performance of LoRA fine-tuned Qwen2-VL models.

Datesets	V7W (ACC)	ST-VQA (ACC)	TextVQA (ACC)	PaintingF (BLEU / ROUGE)	MathV (ACC)
Before fine-tuning	0.8%	29.8%	23.9%	7.6% / 11.9%	7.0%
After fine-tuning	37.9%	47.7%	78.7%	13.4% / 16.2%	66.6%

Table 11. Utility performance of full fine-tuned Qwen2-VL models.

Datesets	V7W (ACC)	ST-VQA (ACC)	TextVQA (ACC)	PaintingF (BLEU / ROUGE)	MathV (ACC)
Before fine-tuning	0.8%	29.8%	23.9%	7.6% / 11.9%	7.0%
After fine-tuning	36.5%	88.8%	78.6%	13.5% / 15.9%	86.0%

tion Answering (VQA). This multi-domain architecture addresses critical gaps in existing resources by enhancing image comprehension and mathematical reasoning capabilities, as shown in Figure 10.

A.3. Fine-tuning setting

For both full and LoRA [18] fine-tuning settings, the detailed training configurations are summarized in Table 8. All LoRA fine-tuned models are evaluated in their merged form. For Qwen2-VL, multimodal downstream task fine-tuning is conducted based on the LlamaFactory [49] project.

A.4. Inference setting

We use “generate” function for LLaVA-1.5’s inference in all experiments. We set inference parameters such as temperature at 0.5, Top-p at 0.5, num-beams at 1, and max-new-tokens at 128. For Qwen2-VL, we use default inference setting with max-new-tokens at 128.

B. Additional Experiments

B.1. Utility of the fine-tuning models

We test the utility performance of our two original MLLMs before and after LoRA fine-tuning on downstream task datasets. For full fine-tuning, we report the utility performance of Qwen2-VL before and after fine-tuning on downstream task datasets. As detailed in Tables 9, 10, and 11 fine-tuning substantially enhanced MLLM performance on target tasks. This indicates that there has been a significant change through fine-tuning the model parameters, demonstrating that fine-tuned models effectively simulate real-world application scenarios. Evaluation was conducted on 5,000 ran-

domly sampled test/validation instances from each dataset. For dataset V7W, ST-VQA, TextVQA, and MathV360k, we computed accuracy (ACC) based on answer correspondence. For the dataset PaintingForm, we evaluated BLEU [29] and ROUGE [23] scores.

B.2. Impact on inference parameter settings

In practical model deployment, the performance of trigger tracing may vary due to the randomization effects caused by the configuration of sampling parameters such as temperature and top-P during downstream model inference. We test two fine-tuned variants of LLaVA-1.5 and Qwen2VL across temperature and Top-p values ranging from 0.1 to 1.0 in 0.1 increments. As shown in Figure 11, the results show that the ASR fluctuation stayed within $\pm 1\%$, confirming that AGDI is resilient to inference randomization, such as sampling parameter variation.

B.3. More multimodal datasets fine-tuned models

Tracking the copyright of models fine-tuned for diverse downstream tasks is essential for strong MLLM copyright protection. To further evaluate our method’s robustness, we conduct validation across five prevalent task domains: remote sensing, medical, scientific, autonomous driving, and finance. Specifically, we select RSVQA [27], DriveLM [35], FinVis [42], PathVQA [17] and SciVerse [16]. The details of these five datasets are as follows:

- **RSVQA** is the first remote sensing VQA dataset constructed by automatically extracting information from OpenStreetMap. It comprises two versions based on low-resolution Sentinel-2 satellite imagery and high-resolution aerial imagery, respectively, and covers five types of



Q: Why does the second computer have fish on the screen?
A: Its screen saver is running.



Q: Where is the image taken?
A: Near to house.



Q: What kind of bus is this?
A: Double decker bus.

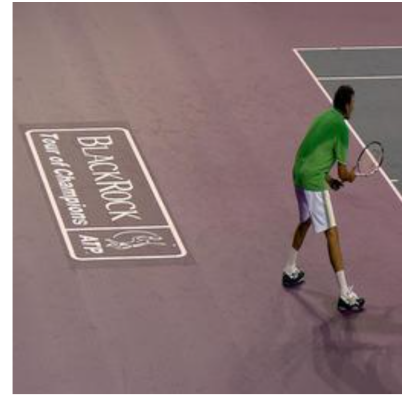
Figure 6. Examples of Visual7W dataset.



Q: What does Espresso sell?
A: Pizza.



Q: What does the writing on the bottom of the picture read?
A: Big Kites.



Q: Who is the sponsor of this tournament?
A: Blackrock.

Figure 7. Examples of ST-VQA dataset.



Q: What letters are embellished on the parachute?
A: Raf.



Q: What man is mentioned on the back of the truck?
A: Ice cream man



Q: What is the last number of the plane?
A: 3.

Figure 8. Examples of TextVQA dataset.

Table 12. Copyright tracking performance on more multimodal downstream models.

Method	Qwen2-VL					InternVL3.5				
	Pathvqa	DriveVQA	FinVis	RSVQA	SciVerse	Pathvqa	DriveVQA	FinVis	RSVQA	SciVerse
Ordinary	41%	52%	50%	55%	69%	30%	27%	26%	36%	46%
RNA	39%	43%	43%	46%	54%	29%	19%	17%	30%	35%
PLA	55%	76%	72%	76%	86%	40%	46%	52%	64%	73%
AGDI	58%	80%	77%	79%	88%	45%	50%	57%	70%	76%

Q: Craft a well-structured paragraph that delves into the formal analysis of visual elements, ensuring a comprehensive exploration of their intrinsic qualities.



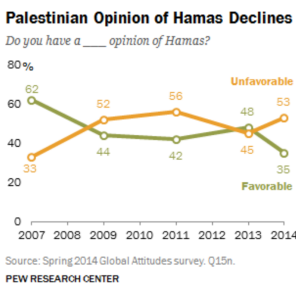
A: This painting showcases a vibrant and colorful composition, with a focus on two round fruits placed prominently in the center of the canvas. The artist's use of bold, expressive brushstrokes creates a sense of movement and energy within the piece, particularly evident in the swirling patterns of light and shadow that dance across the surface of the fruits. The rich, warm tones of reds, yellows, and greens add a sense of depth and dimension to the objects, making them appear almost three-dimensional. The background of the painting is kept relatively simple, with soft, blurred forms that serve to highlight the detailed rendering of the fruits themselves. The play of light and shadow on the textured surfaces of the fruits creates a dynamic interplay of highlights and shadows, adding to the overall sense of realism in the piece. The composition is balanced and harmonious, with the two fruits positioned in such a way as to draw the viewer's eye towards the center of the painting. Overall, this work demonstrates the artist's skill in capturing the beauty and vitality of everyday objects through his masterful use of color, light, and texture.

Q: Craft a well-structured paragraph that delves into the formal analysis of visual elements, ensuring a comprehensive exploration of their intrinsic qualities.



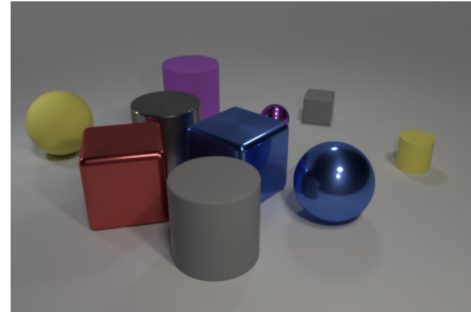
A: The seascape depicts a tumultuous ocean under a dramatic sky. The waves crash against the rocky shore, creating a sense of movement and energy. The sky is filled with dark clouds, which contrast with the bright blue of the water. The use of light and shadow creates a sense of depth and atmosphere. The painting is executed in a realistic style, with attention to detail. The brushstrokes are fluid and expressive, capturing the movement of the waves and the texture of the rocks. The overall effect is one of drama and beauty, as the viewer is drawn into the power and majesty of the sea.

Figure 9. Examples of PaintingForm dataset.



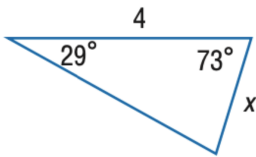
Q: Hint: Please answer the question and provide the final answer at the end. Question: In the year 2014, which opinion is dominant?

A: The answer is Unfavorable.



Q: Hint: Please answer the question and provide the final answer at the end. Question: Subtract all rubber blocks. Subtract all cubes. How many objects are left?

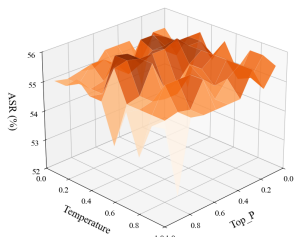
A: The answer is 6.



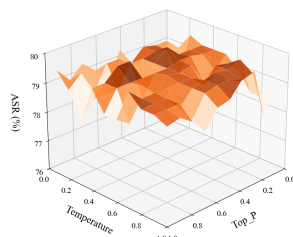
Q: Hint: Please answer the question and provide the correct option letter, e.g., A, B, C, D, at the end. Question: Find x . Round side measure to the nearest tenth. Choices: (A) 2.0 (B) 4.1 (C) 7.9 (D) 8.1

A: The answer is A.

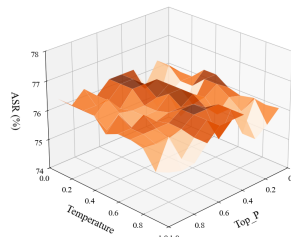
Figure 10. Examples of MathV360k dataset.



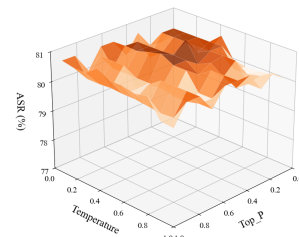
(a) LLaVA-1.5 (ST-VQA).



(b) LLaVA-1.5 (PaintingF).



(c) Qwen2-VL (ST-VQA).



(d) Qwen2-VL (PaintingF).

Figure 11. Hyperparameter analysis results of inference settings (Top-p and temperature). (a)(b) ASR on ST-VQA and PaintingF for LLaVA-1.5; (c)(d) ASR for Qwen2-VL.

question-answer pairs: counting, existence, area estimation, comparison, and urban-rural classification.

- **DriveLM** is a graph-structured VQA dataset for autonomous driving, available in both real-world and simulated versions. By integrating semi-regularized with fully automated annotation, it achieves superior scale, coverage, and logical complexity over existing benchmarks, offering a generalizable platform for training and evaluating vision-language models in autonomous driving domain.
- **FinVis** presents the first two-stage multimodal instruction dataset designed for financial chart analysis. Featuring a pretraining stage for vision-language alignment on historical charts and an innovative instruction-tuning stage that incorporates future data for forecasting, the dataset is structured as image, instruction, answer triplets. It provides comprehensive support for professional tasks including chart description, financial question answering, and trend prediction.
- **PathVQA** is a medical visual question answering dataset derived via a semi-automated pipeline from textbooks and digital libraries. It is designed to simulate the American Board of Pathology examinations, with open-ended clinical questions constituting 50.2% of its content.
- **SciVerse** introduces a multimodal scientific assessment dataset spanning physics, chemistry, and biology. It analyzes LLM capabilities in knowledge, vision, and reasoning by varying the knowledge and visual complexity of the problems. This is paired with a novel scientific CoT evaluation strategy to progressively pinpoint knowledge and logic errors, providing deep diagnostic insights into models’ problem-solving gaps.

In the fine-tuning setup, we employ the full training set for PathVQA, whereas a 30k-sample subset of the training set is used for each remaining dataset. As shown in Table 12, we report the ASR of LoRA fine-tuned variants of Qwen2-VL-2B-Instruct and InternVL3.5-2B-HF. The results demonstrate that AGDI achieves superior copyright tracing performance compared with the baselines across a wide range of multimodal and fine tuning scenarios.

B.4. Experiments on more MLLMs

We also evaluate the copyright tracking performance on the advanced MLLM such as InternVL3.5 [40]. InternVL3.5 is an open-source multimodal model series featuring a "ViT-MLP-LLM" architecture that significantly enhances reasoning capabilities via cascade reinforcement learning and innovatively introduces a Visual Resolution Router (ViR) for dynamic visual token compression together with Decoupled Vision-Language Deployment. We report the ASR on the InternVL3.5-HF 2B and 8B parameter scale models. As shown in Tables 13 and 14, consistent performance confirms that our method generalizes effectively across different architectures and increasing parameter scales. These re-

sults demonstrate that the effectiveness of our method is not limited by model size or architecture, exhibiting strong generalization to fine-tuned models.

Table 13. Copyright tracking performance on InternVL3.5 8B fine-tuned models.

MLLM	Method	V7W	ST-VQA	TextVQA	PaintingF	MathV
InternVL3.5-8B	Ordinary	14%	21%	15%	9%	16%
	RNA	16%	22%	15%	11%	20%
	PLA	44%	55%	46%	31%	49%
	AGDI	58%	63%	62%	45%	58%

B.5. Tracking results under input transformations.

We report the copyright tracing results of our method under several common input level perturbations, including JPEG compression, Gaussian noise, and image resizing, to evaluate the robustness of the generated trigger images. The maximum magnitude of the Gaussian noise is set to 5, and the resized image resolution is fixed at 256. In Table 15, results on LLaVA-1.5 variants demonstrate that our method exhibits robustness against input transformations.

B.6. Ablation study of more parameters

We add the ablation study for parameter λ and fine-tuning epochs in Figure 12. The results in Figure 12a show consistent and stable performance across various λ values, demonstrating the robustness of our method to this hyperparameter. The results in Figure 12b shows that ASR stabilizes with more finetuning, proving increased scale cannot bypass our protection. Our setup aligns with practical scenarios relying on lightweight methods. Furthermore, given the trade-off between cost and utility, aggressive operations like full re-training are impractical because they degrade the model’s performance and commercial value.

B.7. Sensitivity analysis of trigger selection

We provide a sensitivity analysis of trigger selection for copyright tracking performance. Table 16 shows that tracking results depend more on the specific model than the trigger pairs. Furthermore, we use five diverse QA pairs and 200 random images per pair to prevent bias and ensure consistent results on the models.

B.8. Robustness of system prompt variations

In real-world scenarios, malicious users or downstream developers usually modify the system prompt. We test the ASR on the fine-tuned models under system prompt variations. We design two system prompt as follows.

- As a clinical psychologist, use an empathetic tone and prioritize asking questions to guide emotional expression before offering advice.

Table 14. Copyright tracking performance on InternVL3.5 2B fine-tuned models.

Method	LoRA Fine-tuning					Full Fine-tuning				
	V7W	ST-VQA	TextVQA	PaintingF	MathV	V7W	ST-VQA	TextVQA	PaintingF	MathV
Ordinary	25%	38%	32%	12%	23%	35%	38%	30%	21%	30%
RNA	23%	40%	30%	10%	20%	33%	40%	31%	18%	26%
PLA	39%	53%	45%	23%	34%	46%	53%	42%	38%	45%
AGDI	42%	55%	47%	30%	41%	49%	56%	44%	49%	51%

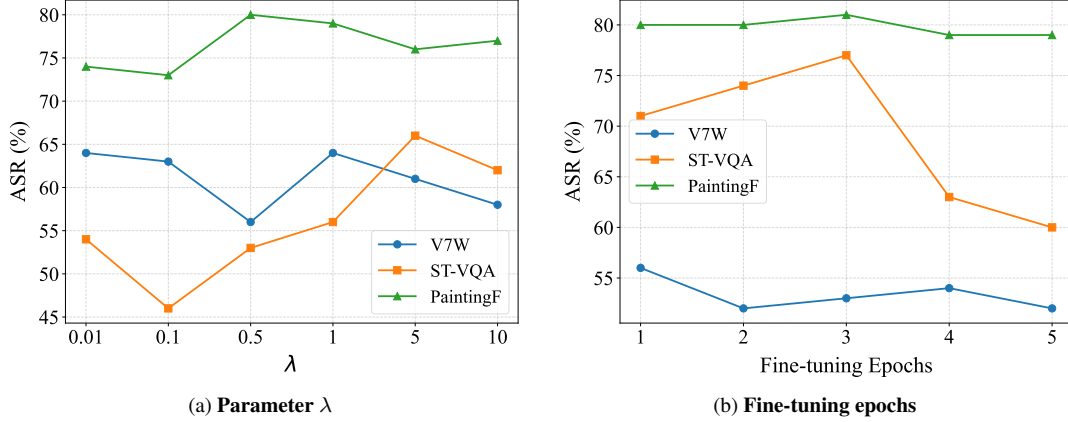


Figure 12. Ablation study for λ and fine-tuning epochs: (a) The impact of loss function parameter λ on tracking performance; (b) The impact of downstream fine-tuning epochs on tracking performance.

Table 15. Copyright tracking under input transformations.

	V7W	ST-VQA	TextVQA	PaintingF	MathV
Original	64%	56%	36%	79%	30%
Resizing	42%	40%	26%	53%	19%
Gaussian	60%	53%	31%	73%	27%
JPEG	40%	39%	24%	42%	16%

Table 16. ASR on 5 different QA pairs.

	QA1	QA2	QA3	QA4	QA5
V7W	63%	75%	70%	68%	37%
ST-VQA	58%	62%	44%	61%	48%
PaintingF	81%	86%	69%	93%	62%

- As a technical interviewer from a top tech firm, evaluate the candidate’s programming basics and provide feedback after each answer.

Table 17 shows consistent ASR across different models before and after system prompt modifications. These results confirm system prompt robustness of AGDI.

B.9. CLIP-like module stability evidence

We measure the similarity drift between 200 triggers and target texts across various fine-tuned models. As shown in Table 18, the minimal cosine similarity drift strongly sup-

Table 17. System prompt experiments on LLaVA-1.5 LoRA variants.

	V7W	ST-VQA	TextVQA	PaintingF	MathV
Original	64%	56%	36%	79%	30%
Sys prompt1	61%	53%	32%	73%	26%
Sys prompt2	63%	54%	32%	74%	25%

Table 18. Average similarity drift(%) on the fine-tuned models.

Similarity drift	Pair1	Pair2	Pair3	Pair4	Pair5
Base→ V7W	4.4%	9.3%	1.0%	2.1%	6.1%
Base→ MathV	6.9%	7.1%	3.3%	0.5%	1.2%

ports the CLIP-like semantic stability assumption, confirming that AGDI’s gains stem from exploiting intrinsic model properties.